THE JOURNAL OF PHYSICAL CHEMISTRY C

Article

pubs.acs.org/JPCC

Over-Speeding Rotational Transmission of a Carbon Nanotube-Based Bearing

Kun Cai,[†,‡] Haifang Cai,[†] Liang Ren,[§] Jiao Shi,[†] and Qing-Hua Qin*[,‡]

[†]College of Water Resources and Architectural Engineering, Northwest A&F University, Yangling, 712100, China

[‡]Research School of Engineering, The Australian National University, Canberra, ACT 2601, Australia

[§]China Petroleum Pipeline Domestic Division, Langfang, 065000, China

Supporting Information

ABSTRACT: In studying the rotational transmission behavior of a carbon nanotube-based bearing (e.g., (5, 5)/(10, 10)) driven by a CNT motor (e.g., (9, 9)) at finite temperature, one can find that the rotor has different dynamic states from the motor at different environmental condition. In particular, the rotor can be in the overspeeding rotational transmission (ORT) state, in which the rotational speed of the rotor is higher than that of the motor. If we change the rotational frequency of the motor (e.g., >100 GHz) and the curved angle of the rotor, the bearing can reach the ORT state. Besides, in the ORT state, the ratio of the rotor's rotational speed over that of the motor will be not higher than the ratio of the motor's radius over that of the rotor. There are two major reasons that result in the bearing to the ORT state. One is that the thermal vibration of atoms between the carbon−hydrogen (C−H) end of the motor and that of the rotor has a drastic collision when the motor is in a high rotational speed. The collision causes the atoms at the end of the rotor to have a circular and axial velocity. The circular velocity leads to the rotation of the rotor and the axial velocity causes the oscillation of the rotor. Another reason is sourced from the oblique angle between the rotor and the stators due to the rotor having a curved angle. A higher oblique angle results in higher friction between the rotor and stator, and it also provides higher collision between the rotor and motor. Hence, one can adjust the transmission state of the rotor by changing not only the environmental temperature but also the rotational speed of the motor, as well as the curved angle of the rotor. The mechanism is essential in guiding a design of a rotational transmission nanodevice which transforms the rotation of the motor into other states of the rotor as output signals.

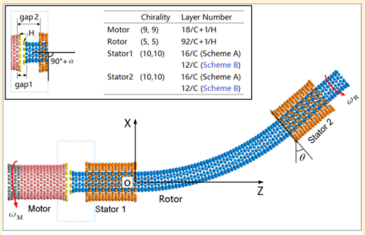

Type	ω_M	Scheme A			Scheme B		
		θ=0°	θ=20°	θ=40°	θ=0°	θ=20°	θ=40°
$\frac{\omega_R}{\omega_M}$	50 GHz	0.99	0.80	0.59	0.95	0.92	0.40
	100GHz	1.21	1.15	0.71	1.19	1.17	0.73
	150 GHz	1.52	1.46	1.12	1.53	1.52	1.17
	200GHz	1.43	1.46	1.10	**1.60**$_{max}$	0.90	0.51
	250 GHz	1.45	1.47	1.42	1.47	***0.00***	1.39
	300GHz	1.23	1.22	1.20	1.12	1.22	1.16

Note: $\frac{\omega_R}{\omega_M} > 1.15$ means the rotor is in an obvious over-speeding rotational transmission state.

1. INTRODUCTION

Nanodevices made from carbon nanotube (CNT) has attracted much attention in recent years,[1−8] due to the excellent mechanical properties of multiple wall carbon nanotubes (MWCNTs), e.g., ∼1 TPa of in-shell modulus[9] and superlubricity between shells and high flexibility.[10,11] The CNT-based nanomotor is, in particular, made so small, e.g., as small as a few nanometers, so that different configurations of the tubes may lead to the motor having different mechanical properties. In 2004, Bourlon et al.[12] investigated the cargo motion of a mass on a CNT bearing under electric force. Barreiro et al.[13] observed the relative motion of the short outer tube on the long inner tube under the axial thermal gradient. Li et al.[14] discussed the sliding behavior between nested MWCNTs and estimated the pull-out force with respect to different walls. Popov et al.[15] investigated the relative motion of a double wall carbon nanotube (DWCNTs) using *ab initio* calculations. Later on, they reported new results on the intertube interactions in DWCNTs with hydrogenated ends and showed that the edge effect in DWCNTs has a great influence on the relative motion between tubes.[16] Guo et al.[17] found that the coupling of van der Waals (vdW) interaction and thermal vibration near the ends induces a high potential edge barrier and edge force, which is stronger than the inter-tube interaction in the mid part of the tubes.

In the work mentioned above, the relative motion involved between tubes is mainly translational. As a matter of fact, the relative motion can also be rotational. For instance, Belikov et al.[18] classified the motions of DWCNTs into rotation, sliding, and spiral motion with respect to such factors as radii difference and chiralities of tubes. Kang and Hwang[19] built a complicated model of rotary nanodevice made from a carbon nanotube oscillator, rotary motor, channel, nozzle, etc. The gas flow produced by the oscillator can also drive the rotation of rotary motor. Bourlon et al.[12] fabricated a nanoelectromechanical system (NEMS) with a plate driven by the external electric field to rotate around a multiwall nanotube bearing. Tu and Hu[20] designed a rotary motor from DWCNTs with a short outer tube on a fixed long inner tube. The rotational of the outer tube was observed when an axially varying voltage was applied. Santamaria-Holek et al.[21] found the rotation in a zigzag/zigzag DWCNTs. As the DWCNTs were made from chiral tubes, the spiral motion could also be observed. In the static electronic field, the charged inner tube in an outer tube can also be actuated to rotate.[5] Recently, we further found that

Received: January 14, 2016
Revised: February 19, 2016
Published: February 23, 2016

DOI: 10.1021/acs.jpcc.6b00420
J. Phys. Chem. C 2016, 120, 5797−5803

the inner CNT in a fixed outer CNT would rotate under a canonical *NVT* ensemble with constant temperature.[6] In particular, the rotational frequency was over 100 GHz. From these studies, one can conclude that a rotary nanodevice can theoretically be produced by the above methods.

Understanding of mechanisms of motion transmission is essential in nanomotor development. Similar to the case of a car, its speed is different from that of the motor. From the rotation of the motor in an engine to the running of wheels, there are many steps to change the rotation states. In the process, the bear-box plays an important role. On the basis of this idea, we proposed the concept of a rotational transmission system.[22] To change the rotational direction, we developed an universal nano joint made from curved CNT.[23] From the results reported there, one may find that the rotational speed of the rotor in the DWCNT-based bearing is never higher than that of the motor. Commonly, the rotor rotates slower than the motor. What shall we do when we need an overspeeding rotational transmission (ORT) system, i.e., where the rotor rotates faster than the motor? To this end, we propose here a rotational transmission system (Figure 1) made from a curved

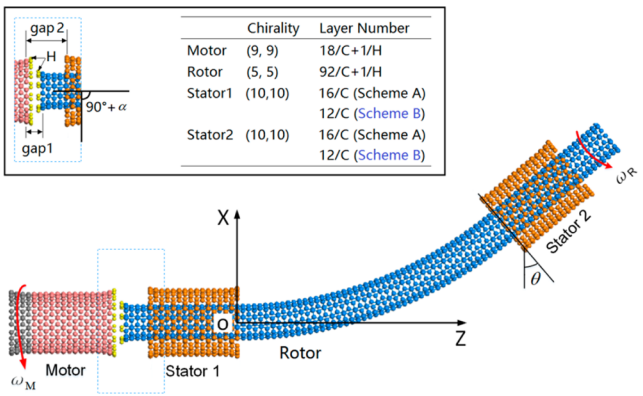

Figure 1. Model of nanodevice made from CNTs obtained by mapping the straight CNTs after energy minimization. The initial value of gap1 is ∼0.113 nm. For either scheme A with 16-layer stators or scheme B with 12-layer stators, the coordinate system, the layout of the motor, the rotor, and the inner ends of the stators are the same. The curved angle of the mid part (50 layers) of the rotor between the inner ends of two stators, θ, is chosen to be 0°, 20°, and 40°, respectively. Gap2 is the axial distance between the right end of the motor and the left end of stator 1. The value of gap2 is 0.85 nm in scheme A and 1.33 nm in scheme B. The different values of gap2 result in different oblique angles, α, between axes of the curved rotor and stator1 at the left side during the rotational transmission.

CNT with chirality of (5, 5) in two of the same stators with a chirality of (10, 10) which is driven by a CNT motor with a chirality of (9, 9). The essential factors, such as the initial distance between the rotator and motor, the length of the stator, the curved angle of the rotor, temperature and the rotational speed of the motor, are involved in the discussion to reveal the mechanism of the ORT.

2. MODEL AND METHODS

In the simulation performed by means of an open-source MD package LAMMPS,[24] the adaptive intermolecular reactive empirical bond order (AIREBO) potential[25] is adopted in calculating the interactions of carbon (C) and/or hydrogen (H) atoms in the system. The time step for integration of Newton's second principle law is 0.001 ps. In simulation, there are four steps in finding the results:

(1) Build the model shown in Figure 1 which (a) creates the straight single-walled CNT for motor and DWCNTs for bearing; (b) performs energy minimization of the tubes; (c) curves the right side of the *Y*-axis (i.e., Z > 0) using the mapping method.[26]
(2) Fix four layers of atoms near the left end of the motor, all atoms on the two stators and four layers of atoms close to the upper-right end of the rotor.
(3) Carry out a Nosé−Hoover thermal bath for the system at a canonical *NVT* ensemble, and make the stage last 400 ps.
(4) Release the motor and rotor after thermal bath and, simultaneously, apply a fixed rotational period (i.e., the reciprocal of the rotational frequency ω_M) on the four layers of atoms near the left end of the motor. And keep the stage conducting for 10 000 ps.

In the simulation, factors such as the input rotational frequency (ω_M), schemes (A vs. B), temperature, and curved angle (θ) are under consideration. The dynamic responses of the rotor, including rotation (ω_R) and oscillation (gap1), are investigated.

3. RESULTS AND DISCUSSION

3.1. The Dynamic Response of the Rotor in Scheme A at 300 K. In the simulation, the value of θ is set to be 0° (straight rotor), 20° and 40°, respectively. The value of ω_M is set to be in the range of [50, 300] GHz with increment of 50 GHz. For simplicity, the concept of rotational transmission ratio of the system is introduced as

$$R_t = \frac{\omega_R}{\omega_M} \quad (1)$$

When the absolute value of R_t is greater than 1.0, i.e., the rotor rotates faster than the motor, the system is in the ORT state.

To demonstrate the rotational transmission results, we classify four types of rotational transmission states as follows.

(1). R_t = 0.0. Failure of Transmission. When the rotor reaches a stable state and keeps R_t = 0.0, the transmission has failed. The stable state is called the failed transmission (FaT) state.

In Figure 2a, there exists no such result. It means that rotational transmission can happen easily.

(2). R_t < 1.0. If R_t < 1.0, the rotor rotates stably slower than the motor. The state is called the reduced transmission (ReT) state.

In Figure 2a, the history (orange) curves of R_t for the case of θ = 40° indicates that the value of R_t is not higher than unity when the rotational speed of the rotor is stable and the rotor is driven by the motor with no more than 100 GHz of input rotational frequency. Simultaneously, as shown in Figure 2b, the oscillation of the rotor exists, but is not obvious, when the rotational frequency of the motor is 100 GHz or less (Movie 1). When the curved angle of the rotor is small, there exists no such phenomenon. Hence, it concludes that the lower rotational transmission occurs easily when the curved angle of the rotor is relatively large. It is obvious that, when θ is large, the oblique angle between the rotor and the motor is also large, which produces higher friction between the rotor and two stators.[26] When the rotational frequency of the motor is small, the interaction between the adjacent ends of the motor and rotor reduces further due to the oscillation of the rotor (gap1).

DOI: 10.1021/acs.jpcc.6b00420
J. Phys. Chem. C 2016, 120, 5797−5803

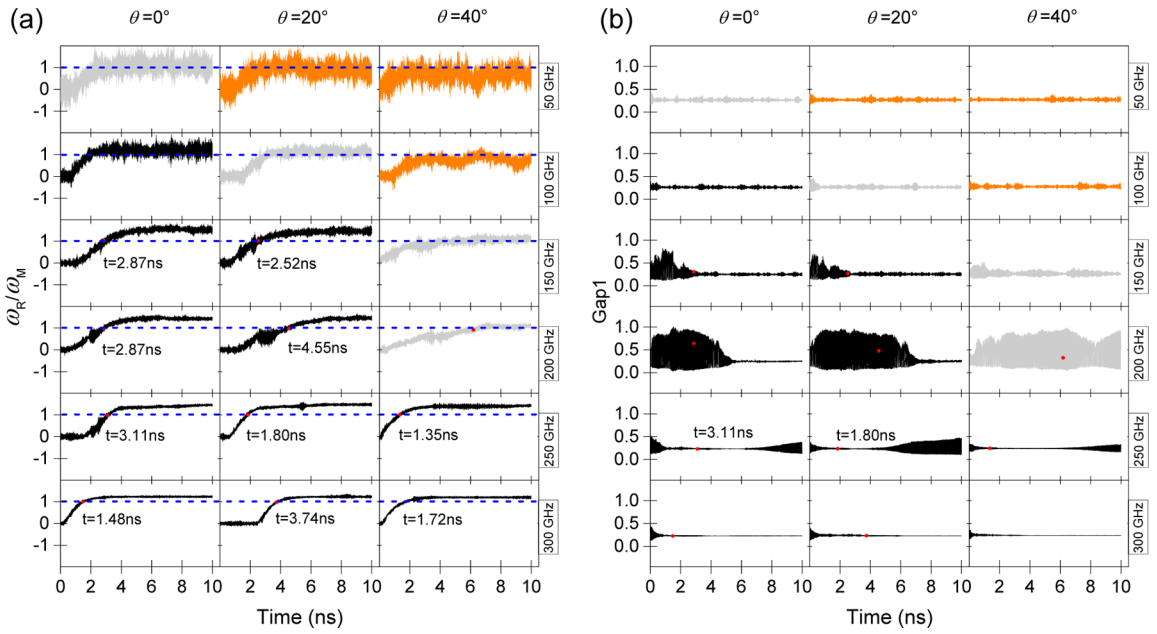

Figure 2. (a) Histories of R_t and (b) histories of gap1 in scheme A with the rotor having different curved angle (0°, 20°, and 40°) and motor having different input rotational frequency (50, 100, 150, 200, 250, and 300 GHz). The time when the system enters the ORT state, i.e., where R_t is greater than 1.0 (exactly 1.15), is labeled. The stable rotational transmission ratios for different cases are listed in Table 1. As the value of R_t is not precisely 1.0, here we suggest the system is in the SyT state when R_t is [0.85, 1.15].

Hence, the low-speed motor cannot drive the large-curved rotor rotate synchronously with it.

(3). R_t = 1.0. In a stable state with R_t = 1.0, the motor and the rotor rotate synchronously. The state is called the synchronous transmission (SyT) state.

In Figure 2a, the four (gray) curves, i.e., the ones for θ = 0° at ω_M = 50 GHz, θ = 20° at ω_M = 100 GHz, θ = 40° at ωM = 150, 200 GHz, demonstrate that the rotational frequency of the rotor increases from zero to that of the motor (Movie 2). In the process, the adjacent ends between the motor and rotor attract each other. The attraction drives the rotation of the rotor. However, the friction between the rotor and the two stators prevents further increase in the rotor's rotational speed. From Figure 2b, one can see that the oscillation of the rotor is also weak. It indicates that the motor and the rotor are "glued" together during rotating (Figure 3a). Hence, the motor with a rotational frequency lower than 200 GHz can drive the rotor rotate not in ORT state but in SyT state instead.

(4). R_t > 1.0. As mentioned previously, when R_t > 1.0, the rotor is in the ORT state. The black curves shown in Figure 2a, indicates that the rotor has higher rotational speed than that of the motor (Movie 3). It obeys the rule that the rotor with higher curved angle in ORT state should be driven by the motor having higher rotational speed. It should be mentioned that the friction between the rotor and the two stators is lower when the rotor has smaller curved angle. From the view of interaction, the rotor is still exerted on with the actuate force by the motor and with the friction force by the two stators. When the rotational speed of the motor is high enough, the interaction between the adjacent ends becomes complicated. For example, the thermal vibration of atoms at the adjacent ends results in obvious radial deviation and the collision between the end atoms on the motor and rotor occurs easily. Thermal vibration of end atoms also increases the relative speed of collision between the motor and rotor. The transient collision can be considered as an elastic interaction between

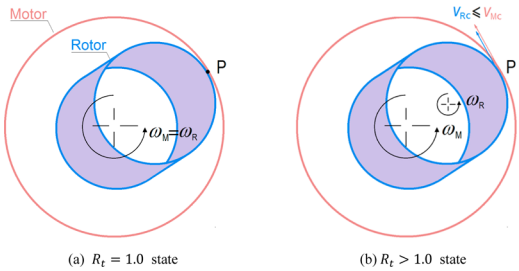

Figure 3. Schematic of mechanism for rotational transmission of the system in different states. (a) SyT state in which the adjacent ends (axial view) are "glued" together at point of tangency (P) and the two tubes rotate around the same axis all the time. Hence, the two tubes rotate synchronously; (b) ORT state, in which the two tubes rotate along their own axes (+), respectively. The velocity vector of point P on the rotor, i.e., $\boldsymbol{v}_R$, is not aligned with that of point P on the motor ($\boldsymbol{v}_M$). Vector $\boldsymbol{v}_R$ has three components along the axial, circular and radial direction, which are labeled as v_{Ra}, v_{Rc} and v_{Rr}, respectively. v_{Ra} will provide axial motion of the rotor; v_{Rc} will result in rotation of the rotor and v_{Rr} produce transversal vibration of the rotor. Commonly, v_{Rc} is not higher than v_{Mc} in average time.

them due to C−H bonds on adjacent ends. Therefore, the end atoms on the rotor obtain a relative high velocity along the circular direction, which provides higher rotational frequency of the rotor due to the radius of the rotor being less than that of the motor (Figure 3b). However, further rotational acceleration of the rotor is confined by the resistance from the two stators. Therefore, we can conclude that the ORT state of the rotor can only be reached when the radius of the rotor is less than that of the motor at a high temperature. Meanwhile, the maximal rotational frequency should be not higher than its ideal transmission frequency:

$$\omega_R \le \omega_R^{Ideal} = \frac{r_M}{r_R}\omega_M \qquad (2)$$

DOI: 10.1021/acs.jpcc.6b00420
J. Phys. Chem. C 2016, 120, 5797−5803

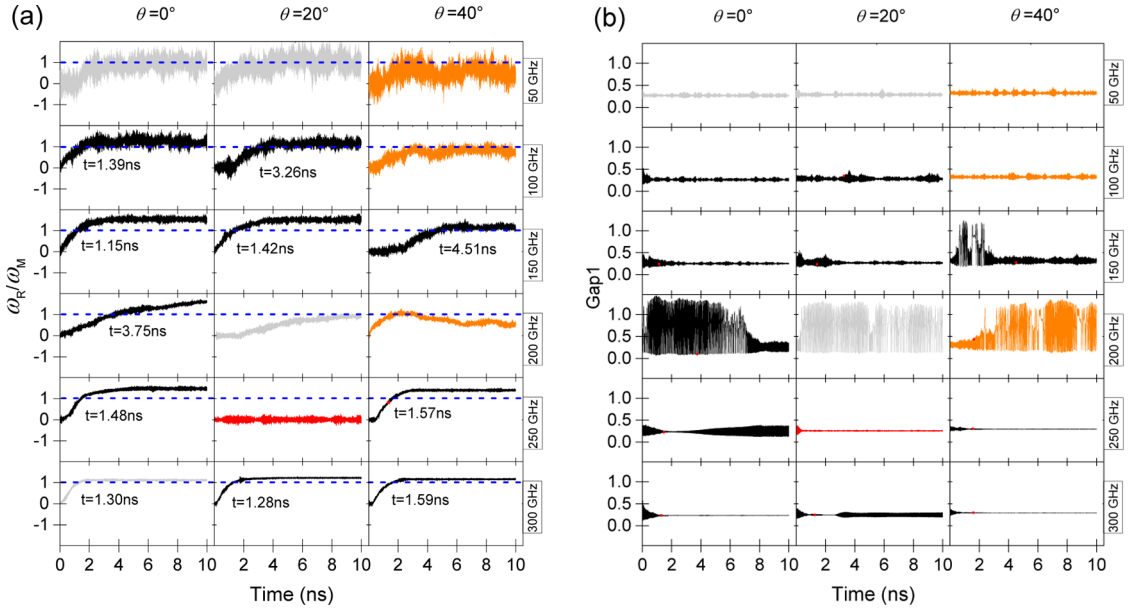

Figure 4. (a) Histories of R_t and (b) histories of gap1 in scheme B with the rotor having different curved angle (0°, 20°, and 40°) and motor having different input rotational frequency (50, 100, 150, 200, 250, and 300 GHz). The time when the system is in ORT state, i.e., R_t is greater than 1.0, is labeled. The stable rotational transmission ratios for different cases are listed in Table 1.

where r_M and r_R are the radii of the motor and the rotor, respectively. ω_R^{Ideal} is the rotational frequency of the rotor with ideal rotational transmission state, i.e., the two adjacent ends are tangent and have no relative sliding, i.e., the linear velocity of the atoms (on the motor and rotor) at the point of tangency are the same. From eqs 1 and 2, one can find the following relationship

$$R_t \leq \frac{r_M}{r_R} \tag{3}$$

In the present simulation, the value of r_M/r_R is 1.8 for the system with (9, 9) motor and (5, 5) rotor. In Figure 2, there is no stable value of R_t that is higher than 1.8.

As one can see that the oscillation of the rotor (history curve of gap1) is very obvious when it is driven by a 200 GHz motor (Figure 2b). When the curved angle of the rotor is small, e.g., 0° or 20°, the oscillation stops after ~5 to 7 ns. However, the rotor with a curved angle of 40° has more stable large-amplitude oscillation (Movie 3). For this rotor, its stable rotational frequency tends to be identical to that of the motor after ~6.20 ns. What is the reason for this? By comparing the oscillation of the rotor shown in Figure 2b, we find that only when the rotational speed of the rotor is close to 200 GHz does the oscillation become obvious. Hence, we consider that 200 GHz should be nearby the eigen frequency of the rotor when it has a stable large-amplitude oscillation while rotating. This phenomenon was found in our previous work.[27] The difference is that the current rotor is a curved tube. It indicates that either straight or curved rotor can be in the state of oscillation with rotation. The eigen frequency changes with the rotor's environment. More discussions are given below.

3.2. Effects of gap2 on the Dynamic Response of the Rotor. In above discussion, the axial distance between the motor and stators, i.e., gap2, is fixed to a value of 0.85 nm in all related simulations (scheme A). Can the rotor behave differently if we only reduce the length of the stator by removing 4 layers of atoms near the outer ends of the two stators? In the present scheme (B), the value of gap2 is 1.33 nm after removing the atoms. Figure 4 shows the rotational transmission results of the system in scheme B at the canonical *NVT* ensemble with T = 300 K.

Comparing Figure 4 with Figure 2, one can see that most results are similar except the following four obvious differences.

(1) In most cases, the rotor reaches the stable rotational state earlier in scheme B than in scheme A. As we know that the oblique angle between the same curved rotor and two shorter stators (in scheme B) is higher. Hence, the free lower-left end of the rotor in scheme B has a higher deflection from z-axis than that in scheme A. The interaction between the adjacent ends of the motor and the rotor becomes stronger and starts earlier in scheme B. Therefore, the rotor reaches the stable state earlier.

(2) Driven by the motor with 200 GHz of rotational frequency, the rotor with a curved angle of 40° is in the ReT state in scheme B while the rotor is in the SyT state in scheme A. By comparing the oscillation of the rotor in both schemes, one can see that the amplitude of oscillation along curved axis is different; e.g., the amplitude in scheme B (Movie 4) is greater than that in scheme A (Movie 3). It may be due to that the oblique angle between the rotor and stator1 in scheme B is larger than that in scheme A. The collision between the adjacent ends of the motor and rotor in scheme B provides higher axial velocity but lower circular velocity of the rotor. Therefore, the amplitude of oscillation increases while the rotational speed drops.

(3) Figure 4b shows that, driven by the motor with 200 GHz of rotational frequency, the rotor with a curved angle of 20° is also in a state of oscillation together with rotation. However, the rotational frequency of the rotor is increasing before 8.5 ns. After 8.5 ns, the rotor is in the SyT state rather than in the ORT state in scheme A. The rotary acceleration of the rotor lasts for a long time.

(4) The FaT state appears when the rotor has a curved angle of 20° and is driven by a 250 GHz motor. One can find

DOI: 10.1021/acs.jpcc.6b00420
J. Phys. Chem. C 2016, 120, 5797−5803

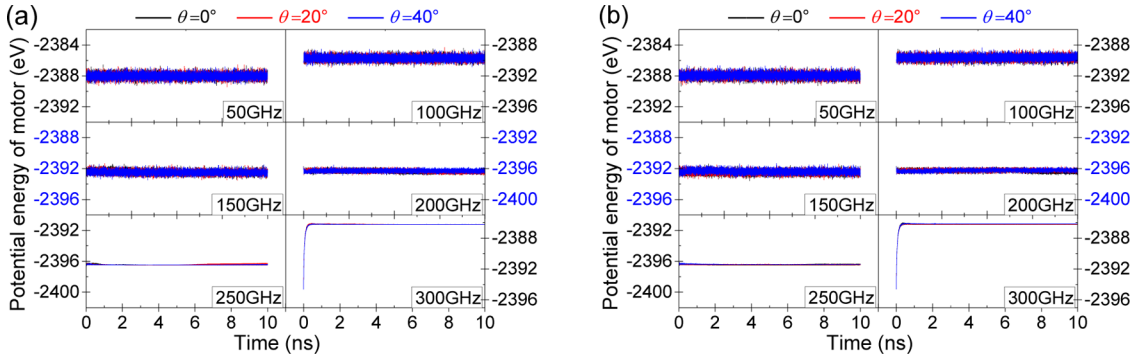

Figure 5. Histories of potential energy of the motor (a) in scheme A and (b) in scheme B when the rotor has a different curved angle (0°, 20°, and 40°) and the motor has a different input rotational frequency (50, 100, 150, 200, 250, and 300 GHz).

Table 1. R_t and the Variation of Potential Energy of the Motor (ΔPE) with Respect to the Initial Value (t = 0)[a]

		scheme A			scheme B		
type	ω_M/ω_R, GHz	θ = 0°	θ = 20°	θ = 40°	θ = 0°	θ = 20°	θ = 40°
R_t	50	0.99	0.80	0.59	0.95	0.92	0.40
	100	1.21	1.15	0.71	1.19	1.17	0.73
	150	1.52	1.46	1.12	1.53	1.52	1.17
	200	1.43	1.46	1.10	1.60_{max}	0.90	0.51
	250	1.45	1.47	1.42	1.47	*0.00*	1.39
	300	1.23	1.22	1.20	1.12	1.22	1.16
ΔPE/eV	50	−1.14	−0.88	−0.69	−1.09	−1.22	−0.20
	100	−2.84	−2.12	−1.88	−2.89	−3.24	−2.35
	150	−5.64	−5.36	−5.21	−5.57	−5.74	−4.69
	200	−9.60	−8.88	−8.48	−9.60	−9.80	−8.98
	250	−9.52	−9.18	−9.13	−9.55	−9.65	−8.58
	300	0.65	1.39	1.58	0.60	0.23	1.11

[a]The values are obtained by statistics over [9.501, 10.000] ns.

that the 20° rotor can be driven to rotate by the motor with any other rotational speed. The reason is mainly due to the edge collision between the motor and rotor cannot provide enough torque to drive the rotor which is simultaneously prevented from the friction between the rotor and stators. The rotational frequency of the motor, i.e., 250 GHz, may be aligned with the breath vibration of the lower left end of the rotor at the present configuration, and the interaction decreases sharply as compared with the motor rotating in other frequencies.

The effect of the other CNT pairs,[22,28] e.g., with different chirality of the motor, rotor, and stators in the model, in the transmission state is not considered due to two reasons. One is that, comparing with zigzag CNT, an armchair CNT is easier to act as an oscillator in the transmission system. The other is that acceleration of the rotor depends slightly on the initial value of gap1 (<1 nm) between motor and rotor. The related discussion can be found in our previous study.[22]

Figure 5 shows the potential energy (PE) histories of the motor. It indicates that the PE of the motor depends mainly on its rotational speed and slightly on the curved angle of the rotor. In brief, the centrifugal force on each atom on the motor becomes stronger when the rotational speed is higher, and the centrifugal force provides higher deformation which needs higher PE in the motor. Hence, from Table 1 we find that the value of PE increase with the rotational frequency in [50, 250] GHz. However, the PE of the 300 GHz motor has a jump (down). It is known that the radius of the motor increases with the increasing of the rotational frequency which provides centrifugal force. At 300 GHz, the motor and the rotor reaches a new equilibrium state which has lower PE. The potential within the bearing changes slightly because of very slight oscillation of the rotor in motor (see Figure 2b and Figure 4b).

Table 1 also demonstrates that the R_t depends slightly on the curved angle of the rotor when it is driven by a high-speed (e.g., 250, 300 GHz) motor in both schemes. R_t reaches its maximal value when the straight rotor in the shorter stators (scheme B) is driven by the 200 GHz motor.

3.3. Temperature Effects on the Dynamic Response of the Rotor. To show the effects of temperature on the output response of the rotor, we compare the results of the model in scheme B with canonical *NVT* ensembles at temperatures of 8, 150, 300, and 450 K (Figure 6). Meanwhile, the input rotational frequency of the motor is set to be 200 GHz, which leads to obvious oscillation of the rotor.

When the environmental temperature is nearly zero, e.g., 8 K, the rotor has neither rotation nor oscillation. As we know, the thermal vibration of atoms on the motor and rotor is negligible at such low temperature. Hence, the atoms are in the ideal shell even if it is in rotating. Hence, the two tubes do not collide strongly enough to produce kinetic energy that maintains the rotation and/or oscillation of the rotor. That is the reason why the rotor is in an FaT state.

At 150 K, thermal vibration of atoms causes enough circular velocity on the rotor. Hence, the curved rotor enters ORT state. However, the rotor oscillates when the rotational state becomes stable. It is interesting that the stable value of R_t is nearby 1.2 for the three curved rotors. In particular, when

DOI: 10.1021/acs.jpcc.6b00420
J. Phys. Chem. C 2016, 120, 5797−5803

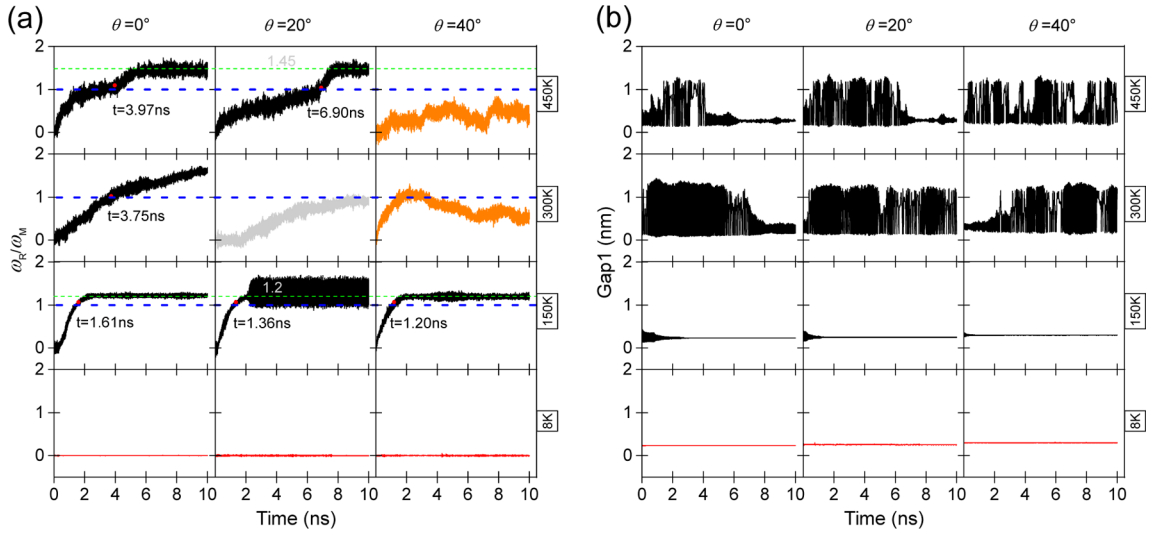

Figure 6. (a) Histories of R_t and (b) histories of gap1 when the curved rotor is driven by 200 GHz motor at different temperature in scheme B. Green dash line represents the stable value of R_t.

θ = 20°, the rotational frequency of the rotor has such characters as large-amplitude and periodic (Movie 5). The value of R_t is between [1.0, 1.6] during rotating.

At 450 K, both rotors with θ = 0° and 20° can be in the ORT state with a stable value of R_t nearby 1.45. The rotors also have slight oscillation after ~7 ns. However, when θ = 40°, the rotor with large-amplitude oscillation is in the ReT state. As comparing with the oscillation of the 40° rotor at 300 K, the amplitude of the present rotor becomes lower at higher temperature. It implies that the drastic thermal vibration of atoms on rotor results in higher friction between the two stators.

For the straight (θ = 0°) rotor, the stable value of R_t can be adjusted by changing the environmental temperature. For the curved (θ = 20° and 40°) rotor, the transmission state can also be varied among the three states, i.e., static, the rotating-only, and the oscillating while rotating. It is significant for the application of the system in a NEMS.

4. CONCLUSIONS

Using MD simulations, we study the dynamic response of a carbon nanotube-based rotational transmission system with a curved rotor constrained by two short stators and driven to rotate by a motor. Some conclusions are necessarily demonstrated for the potential application in the design of a NEMS.

(1) Because of high thermal vibration of atoms on the adjacent ends of the motor and rotor, the collision from these atoms drive the rotation of the rotor. The system can be in four states, i.e., the FaT, ReT, SyT, and ORT states, when we control the environmental temperature and the curved angle of the rotor.

(2) The rotor can be in the ORT state only when the radius of the rotor is less than that of the motor. The maximal rotational transmission ratio is no higher than the ratio of the radius of the motor and that of the rotor.

(3) When the rotational frequency of the motor is lower than 100 GHz, the rotor will be in the ReT or SyT state rather than in the ORT state.

(4) The oblique angle between the curved rotor and the stators determines the interaction between the rotor and other tubes. Constrained by the shorter stators, the oblique angle is higher and the stators provide higher friction to the rotor. Simultaneously, the interaction between the motor and rotor also increases. But the collision of atoms between the motor and rotor provides different velocities along the axis and the circular directions of the rotor. Hence, the oscillation can start easily if the rotor is constrained by shorter stators.

(5) For a rotor with fixed curved angle, the transmission state can be adjusted by changing the environmental temperature. The transmission state can be static (FaT), rotation, and rotation together with large-amplitude oscillation. It is essential for the design of temperature-dependent nanodevices.

■ ASSOCIATED CONTENT

Supporting Information

The Supporting Information is available free of charge on the ACS Publications website at DOI: 10.1021/acs.jpcc.6b00420.

Full captions for the movies. (PDF)

Movie 1: A−300 K−40°−50 GHz−[8.0, 8.2] ns (AVI)

Movie 2: A−300 K−20°−50 GHz−[8.0, 8.2] ns (AVI)

Movie 3: A−300 K−40°−200 GHz−[8.0, 8.2] ns (AVI)

Movie 4: B−300 K−40°−200 GHz−[8.0, 8.2] ns (AVI)

Movie 5: B−150 K−20°−200 GHz−[8.0, 8.2] ns (AVI)

■ AUTHOR INFORMATION

Corresponding Author

*(Q.-H.Q.) E-mail address: qinghua.qin@anu.edu.au.

Notes

The authors declare no competing financial interest.

■ ACKNOWLEDGMENTS

Financial support from the National Natural Science Foundation of China (Grant No. 11372100) is acknowledged.

■ REFERENCES

(1) Han, J.; Globus, A.; Jaffe, R.; Deardorff, G. Molecular Dynamics Simulations of Carbon Nanotube-Based Gears. *Nanotechnology* **1997**, *8*, 95.

DOI: 10.1021/acs.jpcc.6b00420
J. Phys. Chem. C 2016, 120, 5797−5803

(2) Fennimore, A.; Yuzvinsky, T.; Han, W.-Q.; Fuhrer, M.; Cumings, J.; Zettl, A. Rotational Actuators Based on Carbon Nanotubes. *Nature* **2003**, *424*, 408−410.
(3) Wang, B.; Vuković, L.; Král, P. Nanoscale Rotary Motors Driven by Electron Tunneling. *Phys. Rev. Lett.* **2008**, *101*, 186808.
(4) Somada, H.; Hirahara, K.; Akita, S.; Nakayama, Y. A Molecular Linear Motor Consisting of Carbon Nanotubes. *Nano Lett.* **2009**, *9*, 62−65.
(5) Hamdi, M.; Subramanian, A.; Dong, L.; Ferreira, A.; Nelson, B. J. Simulation of Rotary Motion Generated by Head-to-Head Carbon Nanotube Shuttles. Mechatronics. *IEEE/ASME Transactions on* **2013**, *18*, 130−137.
(6) Cai, K.; Li, Y.; Qin, Q. H.; Yin, H. Gradientless Temperature-Driven Rotating Motor from a Double-Walled Carbon Nanotube. *Nanotechnology* **2014**, *25*, 505701.
(7) Wei, Q.; Kang, Y.; Lei, Z.; Qin, Q. H.; Li, Q. A New Theoretical Model of a Carbon Nanotube Strain Sensor. *Chin. Phys. Lett.* **2009**, *26*, 080701.
(8) Qiu, W.; Kang, Y.; Lei, Z.; Qin, Q. H.; Li, Q.; Wang, Q. Experimental Study of the Raman Strain Rosette Based on the Carbon Nanotube Strain Sensor. *J. Raman Spectrosc.* **2010**, *41*, 1216−1220.
(9) Qian, D.; Wagner, G. J.; Liu, W. K.; Yu, M.-F.; Ruoff, R. S. Mechanics of Carbon Nanotubes. *Appl. Mech. Rev.* **2002**, *55*, 495−533.
(10) Cumings, J.; Zettl, A. Low-Friction Nanoscale Linear Bearing Realized from Multiwall Carbon Nanotubes. *Science* **2000**, *289*, 602−604.
(11) Zhang, R.; Ning, Z.; Zhang, Y.; Zheng, Q.; Chen, Q.; Xie, H.; Zhang, Q.; Qian, W.; Wei, F. Superlubricity in Centimetres-Long Double-Walled Carbon Nanotubes under Ambient Conditions. *Nat. Nanotechnol.* **2013**, *8*, 912−916.
(12) Bourlon, B.; Glattli, D. C.; Miko, C.; Forró, L.; Bachtold, A. Carbon Nanotube Based Bearing for Rotational Motions. *Nano Lett.* **2004**, *4*, 709−712.
(13) Barreiro, A.; Rurali, R.; Hernandez, E. R.; Moser, J.; Pichler, T.; Forro, L.; Bachtold, A. Subnanometer Motion of Cargoes Driven by Thermal Gradients Along Carbon Nanotubes. *Science* **2008**, *320*, 775−778.
(14) Li, Y.; Hu, N.; Yamamoto, G.; Wang, Z.; Hashida, T.; Asanuma, H.; Dong, C.; Okabe, T.; Arai, M.; Fukunaga, H. Molecular Mechanics Simulation of the Sliding Behavior between Nested Walls in a Multi-Walled Carbon Nanotube. *Carbon* **2010**, *48*, 2934−2940.
(15) Popov, A.; Lozovik, Y. E.; Sobennikov, A.; Knizhnik, A. Nanomechanical Properties and Phase Transitions in a Double-Walled (5, 5)@(10, 10) Carbon Nanotube: Ab Initio Calculations. *J. Exp. Theor. Phys.* **2009**, *108*, 621−628.
(16) Popov, A. M.; Lebedeva, I. V.; Knizhnik, A. A.; Lozovik, Y. E.; Potapkin, B. V. Ab Initio Study of Edge Effect on Relative Motion of Walls in Carbon Nanotubes. *J. Chem. Phys.* **2013**, *138*, 024703.
(17) Guo, Z.; Chang, T.; Guo, X.; Gao, H. Thermal-Induced Edge Barriers and Forces in Interlayer Interaction of Concentric Carbon Nanotubes. *Phys. Rev. Lett.* **2011**, *107*, 105502.
(18) Belikov, A.; Lozovik, Y. E.; Nikolaev, A.; Popov, A. Double-Wall Nanotubes: Classification and Barriers to Walls Relative Rotation, Sliding and Screwlike Motion. *Chem. Phys. Lett.* **2004**, *385*, 72−78.
(19) Kang, J. W.; Hwang, H. J. Nanoscale Carbon Nanotube Motor Schematics and Simulations for Micro-Electro-Mechanical Machines. *Nanotechnology* **2004**, *15*, 1633.
(20) Tu, Z.; Hu, X. Molecular Motor Constructed from a Double-Walled Carbon Nanotube Driven by Axially Varying Voltage. *Phys. Rev. B: Condens. Matter Mater. Phys.* **2005**, *72*, 033404.
(21) Santamaría-Holek, I.; Reguera, D.; Rubi, J. Carbon-Nanotube-Based Motor Driven by a Thermal Gradient. *J. Phys. Chem. C* **2013**, *117*, 3109−3113.
(22) Cai, K.; Yin, H.; Wei, N.; Chen, Z.; Shi, J. A Stable High-Speed Rotational Transmission System Based on Nanotubes. *Appl. Phys. Lett.* **2015**, *106*, 021909.
(23) Cai, K.; Cai, H.; Shi, J.; Qin, Q. H. A Nano Universal Joint Made from Curved Double-Walled Carbon Nanotubes. *Appl. Phys. Lett.* **2015**, *106*, 241907.
(24) LAMMPS, *Molecular Dynamics Simulator*. (http://lammps.sandia.gov/) 2015.
(25) Stuart, S. J.; Tutein, A. B.; Harrison, J. A. A Reactive Potential for Hydrocarbons with Intermolecular Interactions. *J. Chem. Phys.* **2000**, *112*, 6472−6486.
(26) Cai, K.; Cai, H.; Yin, H.; Qin, Q. H. Dynamic Behavior of Curved Double-Wall Carbon Nanotubes with Rotating Inner Tube. *RSC Adv.* **2015**, *5*, 29908−29913.
(27) Cai, K.; Yin, H.; Qin, Q. H.; Li, Y. Self-Excited Oscillation of Rotating Double-Walled Carbon Nanotubes. *Nano Lett.* **2014**, *14*, 2558−2562.
(28) Hou, Q. W.; Cao, B. Y.; Guo, Z. Y. Thermal Gradient Induced Actuation in Double-Walled Carbon Nanotubes. *Nanotechnology* **2009**, *20*, 495503.

DOI: 10.1021/acs.jpcc.6b00420
J. Phys. Chem. C 2016, 120, 5797−5803